C. R. Physique 3 (2002) 463–478

Solides, fluides : propriétés électroniques et optiques/*Solids, fluids: electronic and optical properties*
(Physicochimie/*Physical chemistry*)

DOSSIER

PHOTONIQUE MOLECULAIRE : MATÉRIAUX, PHYSIQUE ET COMPOSANTS

MOLECULAR PHOTONICS: MATERIALS, PHYSICS AND DEVICES

Organic nanocrystals grown in sol–gel matrices: a new type of hybrid material for optics

Julien Zaccaro [a], Nathalie Sanz [a], Estelle Botzung Appert [a], Patrice L. Baldeck [b], Alain Ibanez [a]*

[a] **Laboratoire de cristallographie, CNRS, UPR 5031 associée à l'Université J. Fourier et à l'INPG, BP 166, 38042 Grenoble cedex 9, France**

[b] **Laboratoire de spectrométrie physique, Université Joseph Fourier, CNRS (UMR 5588), BP 87, 38402 Saint Martin d'Hères cedex, France**

Accepted 1 March 2002

Note presented by Guy Laval.

Abstract We have engineered new hybrid organic–inorganic materials through a simple and generic preparation of stable organic nanocrystals grown in gel–glass matrices. This process is based on the confined nucleation and growth of dyes in the pores of dense gels. For bulk samples, narrow size distributions of particles are obtained between 10 and 20 nm in diameter. We have extended this method to the preparation of organic nanocrystals embedded in sol–gel thin films by spin-coating. For all these nanocomposite samples, we have significantly increased the stability of the dye and obtained promising linear and nonlinear optical properties. ***To cite this article: J. Zaccaro et al., C. R. Physique 3 (2002) 463–478.*** © 2002 Académie des sciences/Éditions scientifiques et médicales Elsevier SAS

confined nucleation and growth / hybrid (organic–inorganic) materials / organic nanocrystals / sol–gel / optics

Nucléation et croissance confinée de nanocristaux organiques en matrices sol–gel : un nouveau type de matériaux organo-minéraux pour l'optique

Résumé Nous avons développé une élaboration simple et générique de nouveaux matériaux hybrides organo-minéraux constitués de nanocristaux organiques inclus dans des matrices sol–gel. Ce procédé est basé sur le contrôle de la nucléation et de la croissance confinée de phases organiques dans les pores de gels denses. Pour les xérogels massifs, nous avons obtenu des distributions de taille de nanocristaux étroites (10–20 nm). Nous avons étendu cette méthode à l'élaboration de couches minces par spin-coating. Dans tous ces matériaux nanocomposites, nous avons stabilisé les phases organiques cristallisées et obtenus des propriétés optiques linéaires et non-linéaires prometteuses. ***Pour citer cet article : J. Zaccaro et al., C. R. Physique 3 (2002) 463–478.*** © 2002 Académie des sciences/Éditions scientifiques et médicales Elsevier SAS

* Correspondence and reprints.
E-mail address: alain.ibanez@polycnrs-gre.fr (A. Ibanez).

S1631-0705(02)01330-0/FLA

nucléation et croissance confinées / matériaux hybrides organo-minéraux / nanocristaux organiques / sol–gel / optique

1. Introduction

Organic phases exhibit unique properties such as luminescence or high nonlinear optical (NLO) efficiency due to the high polarizability of π-conjugated molecules [1]. Moreover, they are associated to unlimited crystal engineering through the great flexibility of their chemical synthesis. In order to take advantage of these properties and to design materials with high quadratic NLO efficiency in the visible and near IR region associated with a convenient stability, a new family of hybrid organic–inorganic crystals has been developed in our laboratory during the last decade [2–6]. These hybrid compounds are the result of a crystal engineering strategy aiming at the production of very cohesive, non-centrosymetric packing of organic polar chromophores by anchoring them onto inorganic subnetworks. The combination of ionic, optically active chromophores with suitable inorganic counterparts leads to acentric three-dimensional networks of short hydrogen bonds. The resulting hybrid crystal structures represent a first compromise between the advantages of the organic phases and inorganic compounds. Indeed, this stategy provided hybrid crystals from convenient crystal growths in solutions leading to bulky crystal morphologies [7–9]. These crystals exhibit a wide transparency range between 0.4 and 1.5 µm, enhanced stabilities (chemical, thermal and mechanical) compared to the corresponding molecular organic crystals and large high quadratic NLO efficiencies [10–13].

This work on crystal engineering and crystal growth of hybrid materials have led us more recently to another strategy based on the confined nucleation and growth of organic phases in the pores of wet gel matrices [14–16]. We selected sol–gel matrices for their high stability, convenient shaping and good optical properties [17]. Moreover, since 1984 [18], it has been extensively shown that the sol–gel method can be used to encapsulate organic molecules in inorganic matrices (bulk or thin films). The flexibility of the sol–gel chemistry based on silicon alkoxide precursors and its ability to prepare stable inorganic matrices close to room temperature are compatible with a wide variety of organic chromophores. Until now, dyes were dispersed within or grafted onto sol–gel networks [18–20]. In our works, the organic phases are aggregated through their confined nucleation in the pores of gel frameworks. This allows us to prepare a new type of hybrid materials constituted of organic nanocrystals grown in amorphous silicate matrices. These nanocomposite compounds not only combine the optical properties of organic phases (luminescence, NLO properties, ...) with those of amorphous inorganic materials (high stability, convenient processing and shaping), but also the advantages of nanocrystals:

- the first advantage of nanocrystals is their small size in comparison to the wavelengths resulting in the preparation of non diffusing samples for visible or IR laser beams;
- secondly, through the nanocrystallization of the dye in the gel–glasses, the chemical stability and photostability of the organic phase are also improved in comparison to isolated molecules dispersed in solutions or in solid matrices such as sol–gel or polymers;
- on the nanometer scale, material properties can be significantly modified by quantum size and surface enhancement effects. In the last two decades, there has been great interest in the enhancement of the optical nonlinearity of metallic (Au, Ag, Fe, ...) and semiconductor (I–VII, II–V and III–V) nanoparticles [21]. This interest is motivated by strong confinement effects on electron–hole excitations, i.e. Wannier excitons. Such effects are not expected in organic crystals where Frenkel excitons are mainly localized on one molecule. This is one of the reasons why the preparation and study of organic aggregates is practically unexplored. However, size effects may also be significant in organic nanocrystals. For example, a confinement of the molecular exchange interactions should lead to an enhancement of the optical nonlinearities [22,23].

Another reason why organic nanocrystals have attracted little attention is the difficulties associated with their processing, shaping and structural characterizations. All the previous and scarse preparations of organic nanocrystals were carried out in the liquid phase [24–27]. Nanocrystals are obtained by the precipitation of saturated dye solutions and are deposited on substrates.

In this paper, we report our main results obtained on a simple and generic preparation of stable organic nanocrystals embedded in dense sol–gel matrices. We firstly present the preparation, characterization and the optical properties of organic nanocrystals grown in bulk gel–glasses. In the second part of this paper, we report on the nanocrystallization of organic phases in sol–gel thin films prepared by spin-coating.

2. Organic nanocrystals grown in bulk gel–glasses

2.1. Preparation of bulk hybrid nanocomposites

2.1.1. *Nanocrystallisation process*

The preparation of organic nanocrystals in bulk gel–glasses is based on the control of the nucleation and growth kinetics of the dye confined in the pores of dense gels. This nanocrystallization method can be decomposed in well-separated steps:

- it starts from homogenous solutions containing a solvent, the organic phase, the silicon alkoxide precursors of the gel and a small amount of water for the hydrolysis of the alkoxides. These solutions are inserted in silica airtight cells and heated at 80 °C in order to rapidly dissolve the dye;
- within a few minutes, transparent sols are obtained, giving, after several hours, wet gels. These gels are then aged for 1–2 days according to the type of sol–gel matrix. This syneresis step allows us to adjust the gel porosity and avoids the formation of cracks during the drying of the samples;
- the nucleation of the organic phase is induced in the pores of the gel which act as nanometer scaled reactors for crystal growth in solution. This nucleation in confined solutions is only possible at very high supersaturations since the mass transport only occurs by diffusion [28,29]. Such high supersaturations are achieved by dropping the temperature from 80 °C to ambient or chilling temperatures. The relative supersaturation, σ, depends on the concentration of organic molecules, their solubility in the solvent and the type of the host matrix. Typically, $\sigma = (c - c_0)/c_0$ is ranging between 1 and 2, where c and c_0 are the actual and equilibrium concentrations, respectively. These very high σ values, at the initial stage of the process, leads to the rapid formation of a high number of organic nuclei in the interconnected pore network of the gel. This burst of nucleation lowers significantly σ, ends rapidly the nucleation step and limits the subsequent growth stage;
- the gels are then slowly dried during several days or weeks, see next section, at room temperature to obtain monolithic xerogels. During this drying step, the growth rate of the nuclei is strongly reduced by the slow diffusion coefficients of molecules in the dense gel matrices;
- finally, the samples are annealed under inert gas (N_2) at temperatures just below the melting point of the dye to improve the crystallinity of the particles. These annealings allow also the removal of the residual solvent and the stabilization of the nanocomposite materials.

Our control of the confined nanocrystallization of the organic phases is based on the diagram established by V. LaMer for the preparation of monodisperse crystals in free solutions [30]. In this later process, nucleation and particle growth should be well separated steps. The dense gel matrices exhibit three main advantages compared to free solutions. The confined nucleation, only possible at very high supersaturations, favors the formation of a single 'burst' of nuclei; the slow growth of the particles, diffusion-controlled, is negligible in comparison to the nucleation rate and finally the gel prevents the nanocrystals from coalescing. The adjusment of the experimental conditions of nanocrystallization are well illustrated by Fig. 1. When a high supersaturation of the organic phase is applied to a gel of low density, just after gelation, the growth rate is too high and leads to dendritic growth, Fig. 1(a). When the nucleation is induced after a synerisis step of a few hours, the matrix is not very dense and the particle growth is not negligible compared to

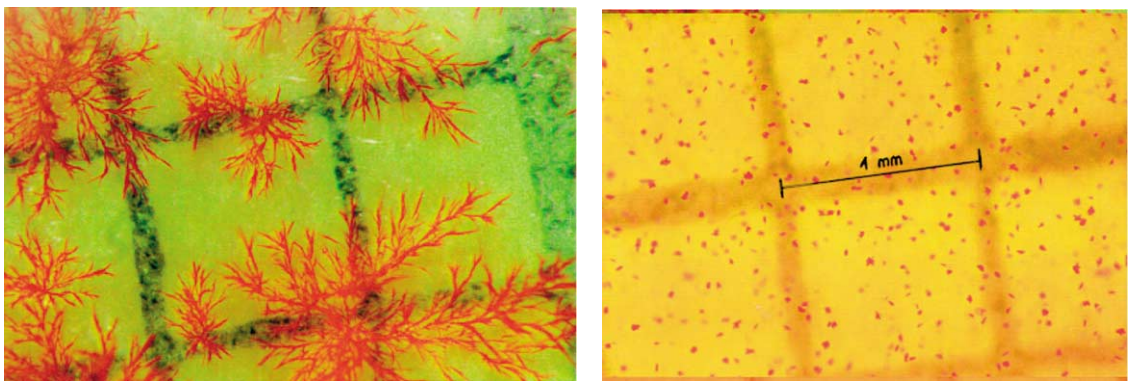

(a) (b)

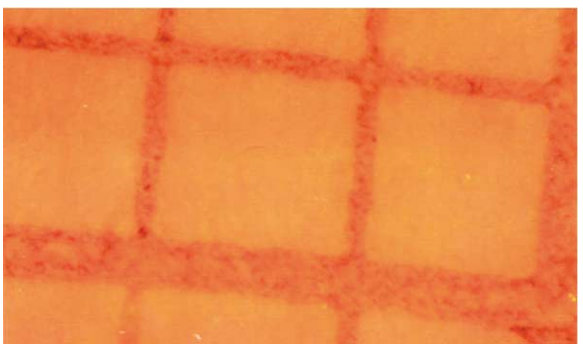

(c)

Figure 1. Nucleation and growth of an organic phase (DEANST) under high supersaturations in wet gels: (a) dendritic growth in a low density gel, just after gelation; (b) microcrystals in a gel obtained after a synerisis of a few hours; (c) nanocomposite sample obtained in a dense gel, 2 days of synerisis.

the nucleation rate. This leads to the formation of polydisperse microcrystals ranging from 20 to 50 µm in diameter, Fig. 1(b). Finally, when the high supersaturation is applied on dense matrices, 1–2 days after gelation, the fast nucleation is well dissociated to the slow diffusion-controlled particle growth. Thus, the original nuclei can grow uniformly when nucleation is over, to yield monodisperse nanoparticles (10–20 nm, see Section 2.2) and transparent samples, Fig. 1(c).

2.1.2. *Sol–gel matrices*

The silicon alkoxides used in this study are listed in Table 1. The first matrices have been prepared from tetramethoxysilane (TMOS) or tetraethoxysilane (TEOS). After these initial experiments, TMOS was selected because its gelation time is shorter than that of TEOS. The resulting silicate network exhibits silanol

Table 1. Silicon alkoxides used in this study

Silicon alkoxides	Chemical formulas	Abbreviations
Tetramethoxysilane	$Si(OCH_3)_4$	TMOS
Methyltrimethoxysilane	$CH_3Si(OCH_3)_3$	MTMOS
Tetraethoxysilane	$Si(OC_2H_5)_4$	TEOS
Methyldimethoxysilane	$CH_3HSi(OCH_3)_2$	MDMS
Polydimethylsiloxane	$HOSi(CH_3)_2[OSi(CH_3)_2]_5OSi(CH_3)_2OH$	PDMS

functions (≡SiOH) which can form hydrogen bonds with the organic molecules. These strong dye–matrix interactions disturb the aggregation of the organic phase (see following sections). In order to minimize these interactions, methyltrimethoxysilane (MTMOS) is added to the TMOS precursor. That way, gel–glasses of high optical quality are obtained from equimolar and 0.4 TMOS + 0.6 MTMOS mixtures. The non-bridging methyl functions, arising from MTMOS, cover the gel pores and screen the silanol functions [31,32]. The resulting Van der Waals bonds between the dye and the sol–gel matrix reduce the dye–matrix interactions and lead to a significant improvement of the nanocrystallization of the organic phase.

The typical polymeric sol–gel matrices are obtained according to procedures available in the literature [17]. Following the nature of the organic molecules involved in the process, different organic solvents have been used such as methanol, ethanol, dioxane, toluene, tetrahydrofuran (THF) or dimethylformamide (DMF) with a molar ratio $s = \text{solvent/alkoxide} = 1$. Gelation of the initial solutions occurs after a few hours in a one step hydrolysis and condensation. These reactions are carried out under acidic conditions (HCl, pH ≈ 1) with 1 H_2O molecule per $–OCH_3$ function ($h = [H_2O]/[OCH_3] = 1$). Neutral conditions have also been used for Lewis's base molecules. In this case, in order to obtain transparent matrices, the TMOS precursor is mixed in equimolar proportions with methyldimethoxysilane (MDMS) which, like MTMOS, has one non-bridging CH_3 function. For the hydrolysis and polycondensation of this 0.5 TMOS + 0.5 MDMS mixture, 0.2 mole of water per mole of $–OCH_3$ function are first added and completed, 24 hours later, until 1 H_2O.

In order to avoid the typical problem of cracks, due to capillary strengths [17] the gels are slowly dried at room temperature from 4 to 6 weeks. In order to reduce significantly this drying period, we have optimized another ORMOSIL (ORganically MOdified SILicate) matrix. We have added to the previous 0.4 TMOS + 0.6 MTMOS matrix a few molar percents of the silicone PolyDimethylSiloxane (PDMS). This silicone involves 14 methyl groups per monomer unit, Table 1. This high number of non-bridging methyl groups leads to a better elasticity of the matrix and to an increase of the pore size of the gel–glasses obtained at the end of the process (xerogel). Indeed, gas adsorption–condensation measurements [33] have shown that the average pore diameter, p, increases with the number of methyl groups pointing towards the inside of the pores: p is centered at 0.6 nm for the TMOS matrix, $p = 1$ nm for the 0.4 TMOS + 0.6 MTMOS matrix and $p = 1.5$ nm when a few molar % of PDMS is added. Thus, both the increase of pore size and elastic modulus of the sol–gel matrices reduce significantly the formation of cracks and the drying duration. Nevertheless, the preparation of this new ORMOSIL, involving several precursors, had to be adjusted to obtain transparent xerogels. We have optimized the precursor molar mixture: 0.57 TMOS + 0.38 MTMOS + 0.05 PDMS. Gelation is carried out under acidic conditions (HCl, pH ≈ 1) with 0.5 H_2O molecule per alkoxide ($–OCH_3$) function ($h = [H_2O]/[OCH_3] = 0.5$). Indeed, the hydrolysis rate and the amount of PDMS have to be small because PDMS is unmiscible with water. Thus, with these ORMOSIL matrices, nanocomposite samples are dried in 5–6 days.

2.1.3. *Organic chromophores*

Different organic molecules have been chosen depending on the targeted optical properties but also to demonstrate the flexibility of our process. In this paper we present results involving nanocrystals of 4-(N, N diethylamino)-β-nitrostyrene (DEANST) and α-[(4′-methoxyphenyl)methylene]-4-nitrobenzene-acetonitrile (CMONS) for their luminescence properties [34,35]. Also, due to the presence of S atoms 4,4 sulfonyldiphenol (SDPH) is used to improve the contrast in transmission electron microscopy (TEM) characterizations [36]. The stilbene 3 laser dye [37] has been selected for its high nonlinear optical absorption while N-(4-nitrophenyl)-(L)-prolinol (NPP) and 3-methyl-4-nitropyridine-1-oxyde (POM) chromophores are used for their quadratic NLO properties [38,39].

The concentration of the organic particles in the final xerogel depends on their solubility and on the nature of the matrix. High doping levels have been achieved with highly soluble chromophores such as SDPH (20 wt%) and stilbene 3 (30 wt%).

2.2. Characterizations of the organic nanocrystals

2.2.1. *Structural characterizations*

The nanocomposite samples are first carrefully observed by optical microscopy. They show a high optical quality without any inhomogeneity at the micrometer scale. This optical quality is confirmed by the lack of significant scattering of laser beams in the micro-Raman and optical studies. On the other hand, no peak associated to nanocrystals are detected by X-ray powder diffraction. The diffraction patterns only exhibit large scattering peaks coming from the amorphous silicate matrix [33]. This is due to the weak scattering factors of the organic phases involved at low concentrations in comparison to the inorganic matrices. Moreover, the small size of nanocrystals induces a broadening of their corresponding diffraction peaks which does not appear above the X-ray scattering of the sample.

The size of the nanocrystals has been determined by coupled studies of transmission electron microscopy (TEM) and small angle neutron scattering (SANS).

TEM experiments are carried out with PHILIPS CM12 and CM30 microscopes working respectively at 120 and 300 kV, in the bright field mode [36]. Since the contrast between amorphous silicate matrices and organic particles is very low, it is enhanced by a slight underfocus. Electron diffraction experiments cannot be achieved because the cristallinity of organic particles is immediately damaged by the electron beam focused on these particles at high magnification [40]. The samples, deposited on holey carbon coated grids, were 100 nm thick slices obtained with an ultramicrotome (LEICA Ultracut SE) equipped with a diamond knife and cooled by liquid nitrogen at 80 K. Figure 2 shows a typical TEM image where one can observe well defined SDPH nanocrystals in a 0.57 TMOS + 0.38 MTMOS + 0.05 PDMS sol–gel matrix, their diameter ranging between 12 and 23 nm. They appear bright in the TEM photographs as their electron density is lower than that of the silicate matrix. In addition to the narrow size distribution, SDPH nanocrystals appear well dispersed as the gel–glass avoids their coalescence.

SANS experiments were carried out on the D11 beam line of the ILL center in Grenoble. Figure 3 shows a typical neutron scattering curve recorded for the same sample of that used in TEM, Fig. 2 (SDPH nanocrystals in a 0.57 TMOS + 0.38 MTMOS + 0.05 PDMS matrix). The main remarkable feature is the presence of a hump located around $Q \approx 0.025$ Å^{-1}. This correlation peak, which corresponds in direct space to distances ranging between 12 and 30 nm, supports the TEM observation. A deeper analysis of these SANS results will be presented elsewhere [33].

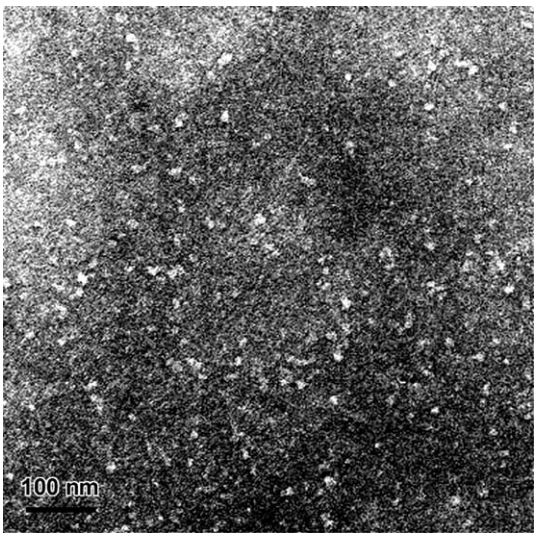

Figure 2. TEM image showing organic nanocrystals of SDPH grown in a 0.57 TMOS + 0.38 MTMOS + 0.05 PDMS sol–gel matrix. The nanocrystals size is ranging between 12 and 23 nm in diameter.

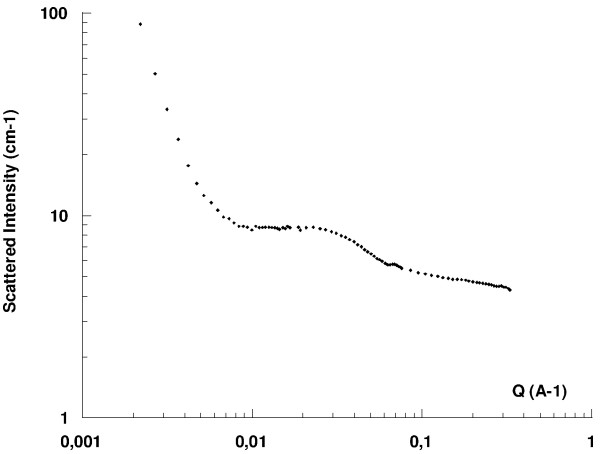

Figure 3. SANS curve registered for SDPH nanocrystals grown in a 0.57 TMOS + 0.38 MTMOS + 0.05 PDMS sol–gel matrix.

2.2.2. *Thermal stability*

Melting peaks are clearly observed for all the nanocomposites samples on differential scanning calorimetry (DSC) curves as illustrated by the case of POM, Fig. 4. This demonstates the crystallinity of the organic aggregates grown in amorphous silicate matrices which are very stable in this range of temperatures. Depending on the chemical reactivity of the chromophore with the silicate matrix, the thermal stability of the nanocrystals grown in gel–glasses can be significantly lower (SDPH), rather similar (CMONS) or significantly higher (NPP, POM, Fig. 4), than the melting temperature of the bulk organic crystals, Table 2.

These results can be explained by the following equation which globally describes the observed size-dependent melting of both free-standing and embedded nanocrystals [41,42]:

$$T_{\mathrm{m}}(r)/T_{\mathrm{m}}(\infty) = \sigma^2(\infty)/\sigma^2(r) = \exp\bigl[-(\alpha-1)/(r/r_0-1)\bigr], \tag{1}$$

where $T_{\mathrm{m}}(\infty)$ is the normal (bulk) melting point of the dye, $T_{\mathrm{m}}(r)$ is the melting point of nanocrystals of radius r, $\sigma^2(\infty)$ and $\sigma^2(r)$ are the averaged mean-square displacement (msd) of atoms or molecules for the bulk crystals and for nanocrystals, respectively. α is the ratio between the msd of atoms at the surface and within the nanocrystal: $\alpha = \sigma_{\mathrm{S}}^2(r)/\sigma_{\mathrm{V}}^2(r) \approx \sigma_{\mathrm{S}}^2(\infty)/\sigma_{\mathrm{V}}^2(\infty)$. r_0 is a critical radius at which all the molecules are located on the surface.

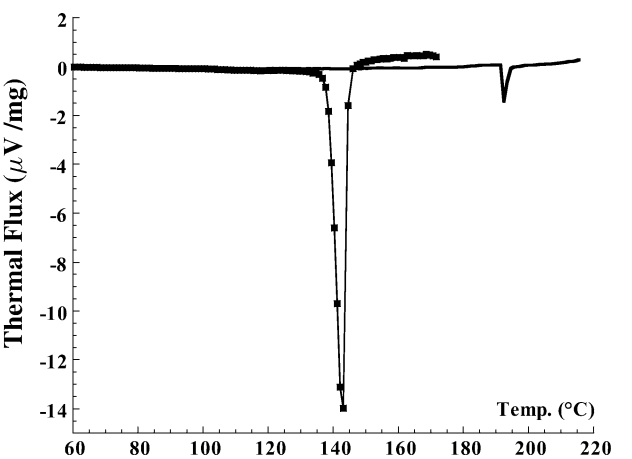

Figure 4. DSC curves of POM powder (squares) and POM nanocrystals grown in a 0.57 TMOS + 0.38 MTMOS + 0.05 PDMS gel–glass (solid curve). The weak intensity of the melting of nanocrystals is due both to the lower dye concentration referred to the POM powder and to the high thermal insulating properties of the gel–glass matrix.

Table 2. Experimental conditions of the preparation of hybrid nanocomposite samples (precursors, organic solvents and dye concentrationds) and the melting points of the organic phases (powder and nanocrystals)

Samples	Solvents	d = [orga]/[alkoxides]	Melting points (T_m °C)	ΔT (°C)
SDPH powder	–	–	247	–
SDPH/TMOS + MTMOS	ethanol	$6 \cdot 10^{-2}$	190	−57
CMONS powder	–	–	163	–
CMONS/TMOS + MTMOS	dioxane	$4 \cdot 10^{-3}$	178	+15
NPP powder	–	–	116	–
NPP/TMOS + MTMOS	acetonitrile	$7 \cdot 10^{-2}$	167	+51
POM powder	–	–	138	–
POM/TMOS + MTMOS + PDMS	acetonitrile	$5 \cdot 10^{-2}$	194	+56

ΔT is the temperature difference between the melting point of the dye powder and that of the corresponding nanocrystals.

Thus, when the molecules at the nanocrystal surface exhibit weak interactions with the matrix, $\sigma_S^2(r) > \sigma_V^2(r)$, $\alpha > 1$ and $T_m(r) < T_m(\infty)$. This is the case in our study of the SDPH nanocrystals (Table 2) where the dye–matrix interactions are mainly Van der Waals bonds. On the contrary, when the atoms at the nanocrystal surface are strongly linked to the matrix, $\alpha < 1$ and $T_m(r) > T_m(\infty)$. This is the case of CMONS, NPP and POM chromophores (Table 2) which can form short H-bonds, particularly between their nitro groups and the silanol functions of the silicate network. These strong dye–matrix interactions, carefully characterized by Raman and NMR spectroscopies [43], explain through Eq. (1) ($\alpha < 1$) why the melting temperature of CMONS, NPP and POM nanocrystals are significantly above the corresponding bulk melting points. Thus, the thermal stability of organic nanocrystals can be greatly improved by the confined growth of the dye in the pores of a dense sol–gel matrix. Nevertheless, if the dye–matrix interactions are too strong, the molecule aggregation and the crystalline structure of the resulting nanocrystals can be significantly disturbed [15,36], see Section 3.2.

2.3. Optical properties of bulk nanocomposite samples

2.3.1. *Luminescence spectroscopy*

The CMONS phase, which exhibits strong luminescence between 500 and 600 nm in the solid state, has three polymorphs characterized by the position of their emission band [34]. As part of this work, we examined the polymorph selectivity and particularly the influence of the sol–gel matrix on the structure of CMONS nanocrystals. Figure 5 shows normalized luminescence spectra recorded for CMONS nanocrystals grown in gels in various solvents. The location of the emission maximum depends on the polymorph which grows from each solvent. The nanocrystals grown in THF correspond to the polymorph CMONS-*a* and have an emission peak centered at 495 nm, nanocrystals obtained from ethanol are CMONS-*c* (emission band around 550 nm) while a mixture of *a* and *c* crystal forms is observed when the solvent is dioxane (Fig. 5). On the other hand, the CMONS-*b*, which is always obtained from the melt, was not observed in gels, even for samples annealed above the melting point.

In addition, we have obtained significant differences in the polymorphism of CMONS crystals obtained from free solutions, and that of nanocrystals grown with the same organic solvents in sol–gel matrices [44]. These results show that both solvent and the silicate network strongly influence the polymorphism of CMONS. The control of the polymorphism through the gel–glass matrix would allow one to adjust the luminescence properties of the nanocomposite organic–inorganic materials. In addition, the CMONS-*a* polymorph, which exhibits a high quadratic NLO efficiency, can be well stabilized in gel–glasses on the contrary to free solutions [44].

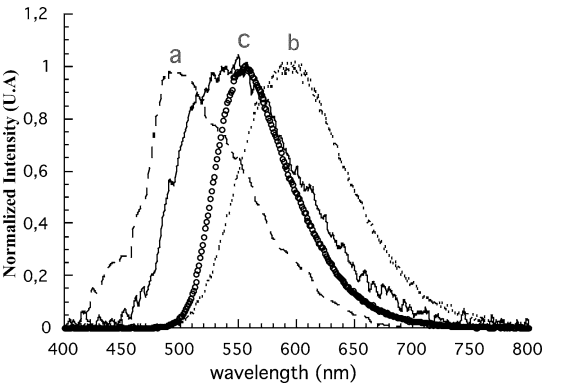

Figure 5. Normalized luminescence spectra of CMONS nanocrystals grown in gel from THF (dotted line), dioxane (solid curve) and ethanol (circle line). Dotted line is the emission band of CMONS-*b* powder obtained from the melt, a, b, and c specify the emission band position of the different CMONS polymorphs.

2.3.2. *Nonlinear absorption for optical power limiting properties*

We have characterized these bulk nanocomposites materials in term of their nonlinear absorption for optical limiting applications. Optical power limiters are needed to protect eyes or photo-detectors from damage caused by tunable laser beams [45]. Ideal materials for this purpose are transparent over the whole visible range of the spectrum at low energy and absorbent for microjoule pulse energy. Materials involving two photon absorption (TPA) satisfy this first requirement with an instantaneous response and no saturation [46], but their nonlinear absorption is too low. This drawback can be overcome in the laser nanosecond regime by combining TPA with excited state absorption. This is the so-called three-photon absorption [37,47]. We have previously reported on the application of organic crystals for TPA where absorption is enhanced through packing effects: high concentration and high local field factor. However, the resulting single crystal devices exhibit a strong anisotropy of response with respect to the laser beam polarization [48]. To overcome this major problem while retaining the high nonlinear absorption of organic crystals, we have characterized the nonlinear absorption of organic nanocrystals which are randomly oriented in the amorphous matrices.

The stilbene 3 laser dye has been selected for its high three-photon absorption efficiency in solution [37]. Optical limiting experiments have been carried out by using a beam waist of $\omega_0 = 35$ µm (HW1/e^2) and a pulse duration of 2.6 ns (FWHM) (Fig. 6). At low energy (less than 5 µJ) the sample is transparent, and the output energy increases linearly with input energy. At higher incident energies, the output energy saturate due to the three-photon absorption of the sample. In this experiment, the output energy is clamped below 20 µJ for all the visible wavelengths. Lower limiting levels can be achieved by decreasing the waist of the incident laser beam. Efficient optical-limiting properties in the visible region have been demonstrated using a F/5 optical system in collaboration with THOMSON LCR and with the support of the French

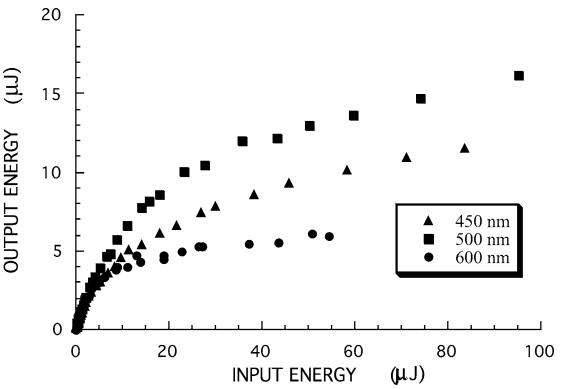

Figure 6. Optical limiting curves obtained for stilbene 3 nanocrystals at several wavelengths in the visible region.

DGA. Thus, a CCD camera has been protected by the nanocomposite samples against shots from a high power nanosecond laser. This new type of hybrid material, which exhibit a good photostability, is a good alternative both to concentrated solutions, due to their stability, and to crystal devices, due to their isotropic response with the laser polarization.

2.3.3. *Quadratic nonlinear optical properties*

We have prepared nanocrystals embedded in gel glasses from POM and NPP molecules, which are known to exhibit high quadratic nonlinear responses in bulk crystals [38,39]. In order to reach new optical properties with our nanocomposites materials, such as quadratic nonlinear optics or electro-optics, we have tried to control the nanocrystals orientation during the elaboration process. We have used a high magnetic field, $\vec{H} = 16$ T (superconductive coil) as previous works have demonstrated that organic crystals can be oriented in solution by a magnetic field through their diamagnetic susceptibility [49–52].

NPP samples elaborated with and without magnetic field have been first compared using DSC, Raman and luminescence spectroscopies. These coupled studies show that $\vec{H}$ favors dye aggregation and improves the crystalline quality of the resulting organic particles by reducing the orientation freedom of molecules and clusters through cooperative effects of diamagnetic susceptibility [53].

The quadratic NLO study shows for the samples containing POM nanocrystals that whatever the preparation conditions, with and without magnetic field, second harmonic generation (SHG) is not detected. On the contrary, the NPP nanocomposite samples display a weak and inhomogeneous SHG response while a stronger SHG intensity is observed when $\vec{H}$ is applied during the nanocrystallization. In addition, in the latter case, the SHG intensity is found to depend strongly on the propagation direction $\vec{k}$ and polarization of the incident beam compared to $\vec{H}$ (Fig. 7). When $\vec{k}$ is orthogonal to $\vec{H}$, the SHG intensity is high with clear maxima for polarizations perpendicular to $\vec{H}$, along the Y axis. When $\vec{k}$ is collinear to $\vec{H}$, the SHG response is weak and more inhomogeneous throughout the sample. These results demonstrate that $\vec{H}$ influences strongly the orientation of the NPP nanocrystals.

Considering that none of the samples containing POM nanocrystals show any SHG efficiency, a mechanism responsible for the formation of self-oriented domains can be proposed. Indeed, the POM molecule has almost no permanent dipole moment [38] whereas NPP displays a dipole moment of 7D [39,54]. When aggregated in polar structures, these molecular dipole moments will add constructively, leading to nanocrystals with strong dipole moments for NPP and no dipole moments for POM. Hence, NPP nanocrystals, unlike POM nanocrystals, can develop dipole-dipole interactions leading to the formation of self-oriented domains. This formation of self-orientated domains based on the dipole moment of nanocrystals explains the weak SHG signal detected for NPP nanocrystals prepared without magnetic field. On the other hand, when a high magnetic field is applied, the SHG intensity of NPP nanocrystals increases significantly. Indeed, by reducing the orientation freedom of nanocrystals, $\vec{H}$ favors the dipole–dipole

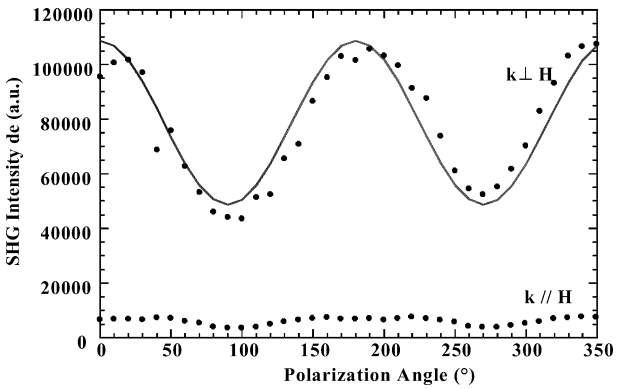

Figure 7. SHG polarization analysis of NPP nanocrystals grown in 0.57 TMOS + 0.38 MTMOS + 0.05 PDMS gel–glass for propagation directions parallel and perpendicular to the magnetic field applied during the nanocrystallization.

interactions and the formation of oriented domains of nanocrystals. This self-orientation phenomenon has to be further investigated in order to better understand this mechanism. Moreover, the nanocrystal orientation will be certainly favored through the strength reduction of dye–matrix interactions by involving other types of gel–glasses. Moreover, work is in progress to better control the orientation of nanocrystals by using high electric fields.

3. Nanocomposites thin films

3.1. Nanocrystallization of organic phases in sol–gel thin films

Recently, we have extended our nanocrystallization process of organic phases in sol–gel matrices to the preparation of nanocomposite thin films [15]. These coatings are deposed by spin-coating on several types of substrates such as microscope slides, silicon wafers or polymers. As for the preparation of monolithic samples the mixtures of silicon alkoxydes, solvent, water and the organic phase are first inserted in airtight containers and heated for about 10 hours at 80 °C in order to obtain homogeneous sols. The sols are then aged during several days at room temperature. This aging step is necessary to obtain high quality films, to ensure the control of particle growth and to avoid the coalescence of the nanocrystals.

In the preparation of organic nanocrystals grown in bulk silicate matrices, matrix gelation, nucleation and particle growth are well separated steps. However, for the thin film process, nucleation and growth of the organic phase begin in the viscous sol at the first stage of the coating process, when the drops of solution are spread out on the substrate. The fast evaporation of the solvent induces instantaneously a high supersaturation of the dye which is associated with the polycondensation of the silicate framework. Thus, we have a one step process since nucleation and growth of the organic particles occurs simultaneously with the formation of the sol–gel matrix which avoids the coalescence of the organic nanocrystals. The coatings are then stabilized by annealing under inert gas at temperatures just above the melting point of the dye.

This preparation of nanocomposite coatings involves strong coupling effects between the elementary processes of this method: nucleation and growth of the organic particles and polymerization of the silicate matrix. Preparing monodisperse particules requires a high control of these coupling effects. A wide distributions of particle size arise generally from nucleation over a relatively long period of time, when young nuclei are produced during the growth of older nuclei. Here we take advantage of the very high supersaturation achieved through the rapid evaporation of the organic solvent. This evaporation induces the germination of a high number of nuclei. This instantaneous nucleation quickly lowers the concentration of the molecularly dispersed dye below the critical concentration for self-nucleation, so only a single ‘burst’ of nuclei occurs leading to narrow size distributions of nanocrystals.

Processing of nanocomposite coatings is mainly controlled by the nature of the sol–gel precursors, the dye concentration, the nature and volatility of the solvent and finally by the rotation speed of the spin-coating apparatus. As for the preparation of bulk samples, we have first used TMOS and TEOS silicon alkoxides (Table 1). We have then particularly selected the equimolar mixture of TMOS + MTMOS. Indeed, as for bulk samples, the non-bridging methyl substituents of MTMOS cover the gel pores and facilitates the dye aggregation as illustrated in the next section. The hydrolysis and polycondensation reactions are acid catalyzed (HCl) with $h = [H_2O]/[-OCH_3] = 1$. Depending on the organic phase, methanol, ethanol, 1,4-dioxane, ethyl acetate or THF is used as solvent with the molar ratio $s =$ solvent/alkoxide $= 3$–6. This molar ratio, directly related to the viscosity of the initial sols, is adjusted to achieve the good nanocrystallization conditions and the preparation of high quality coatings [15]. As for the preparation of bulk nanocomposite samples, in order to demonstrate the validity and the flexibility of this nanocrystallisation process, we have grown nanocrystals of several organic phases such as DEANST and CMONS chosen for their luminescent and nonlinear optical properties [34,35], NPP for its high quadratic NLO efficiency [38] and the pyrido-spiropyran (PSP) for photochromism properties [55]. We have also grown other types of nanocrystals such as naphthalene to demonstrate in this case the gain in stability of the organic phase through the nanocrystallisation process as the naphthalene pure crystals

exhibit a high sublimation rate. The concentration of the organic phase depends on its solubility in the corresponding solvent and on the nature of the host matrix. The doping level is expressed as the molar ratio $d = \text{organic/alkoxide} \approx 10^{-2}$–$10^{-1}$. The viscous sols are spread on the substrates by spin-coating with rotation speeds between 1000 and 4000 rpm. In this way, films of 0.7–1.3 µm thickness are prepared. We have adjusted the experimental conditions to obtain particles of sizes ranging between 100 and 500 nm in order to facilitate their observation by optical confocal microcopy.

3.2. Characterizations of the nanocomposite coatings

Optical confocal microscopy has allowed the directly observation of the organic particles by fluorescence or reflection imaging. We have used a confocal scanning microscope because it allows us to eliminate the out-of-focus blur and exhibit an improved lateral (0.2 µm) and axial resolution (0.8 µm). The images presented here were obtained by recording the fluorescence of the DEANST nanocrystals (centered at $\lambda = 640$ nm) excited with a He–Ne laser ($\lambda = 633$ nm). As we will see, they clearly evidence the influence of the different elaboration parameters (matrix type, dye concentration $d, \ldots$) on the nanocomposite coatings.

For example, Fig. 8 displays confocal microscope images of DEANST nanocrystals grown in spin coated films using ethanol as solvent. When TMOS is the only gel precursor used (Fig. 8(a)) the DEANST luminescent particles in the coatings are not as well-defined as when MTMOS is added (Fig. 8(b)). This is due to the non-bridging methyl functions of the host matrix, originating from MTMOS alkoxide, which lower the strength of dye–matrix interactions and hence favor the aggregation. Thus, well-dispersed particles with narrow size distributions, between 200–300 nm in Fig. 8(b), are obtained with equimolar TMOS + MTMOS coatings.

On the other hand, when the rotation speed of the spin-coating apparatus is increased, the rate of solvent evaporation is raised. Thus, the supersaturation applied on the organic phase and the formation rate of the gel framework increase. This decreases the process duration and leads to smaller particle sizes and narrower

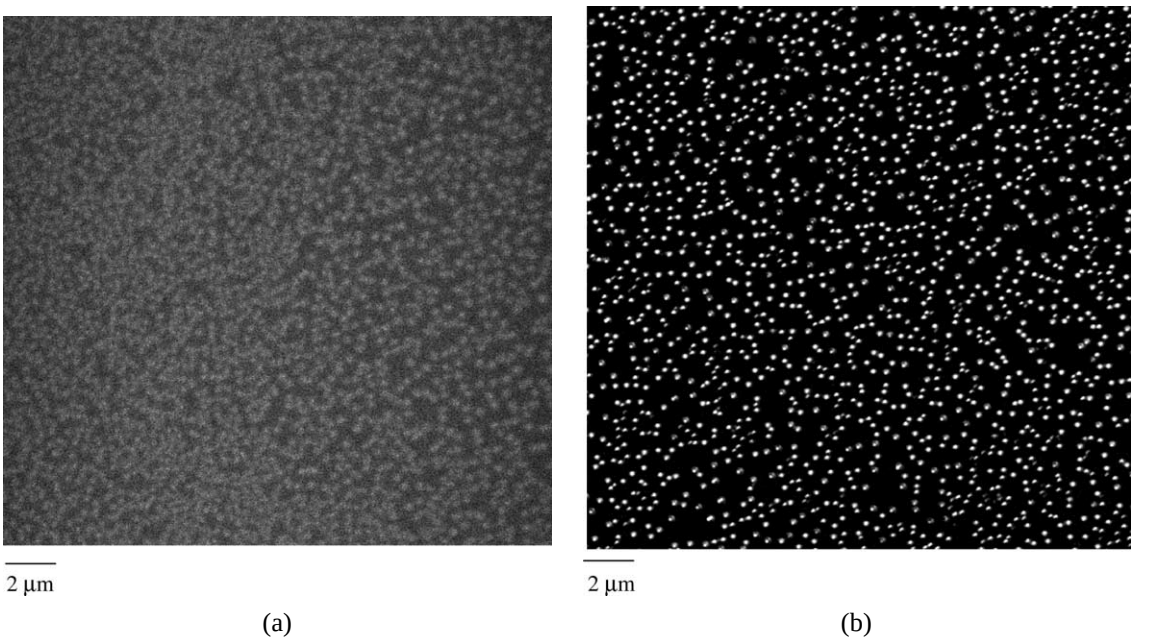

Figure 8. Confocal microscope images of DEANST nanocrystals grown with ethanol in TMOS (a) and TMOS + MTMOS (b) sol–gel thin films (fluorescence imaging).

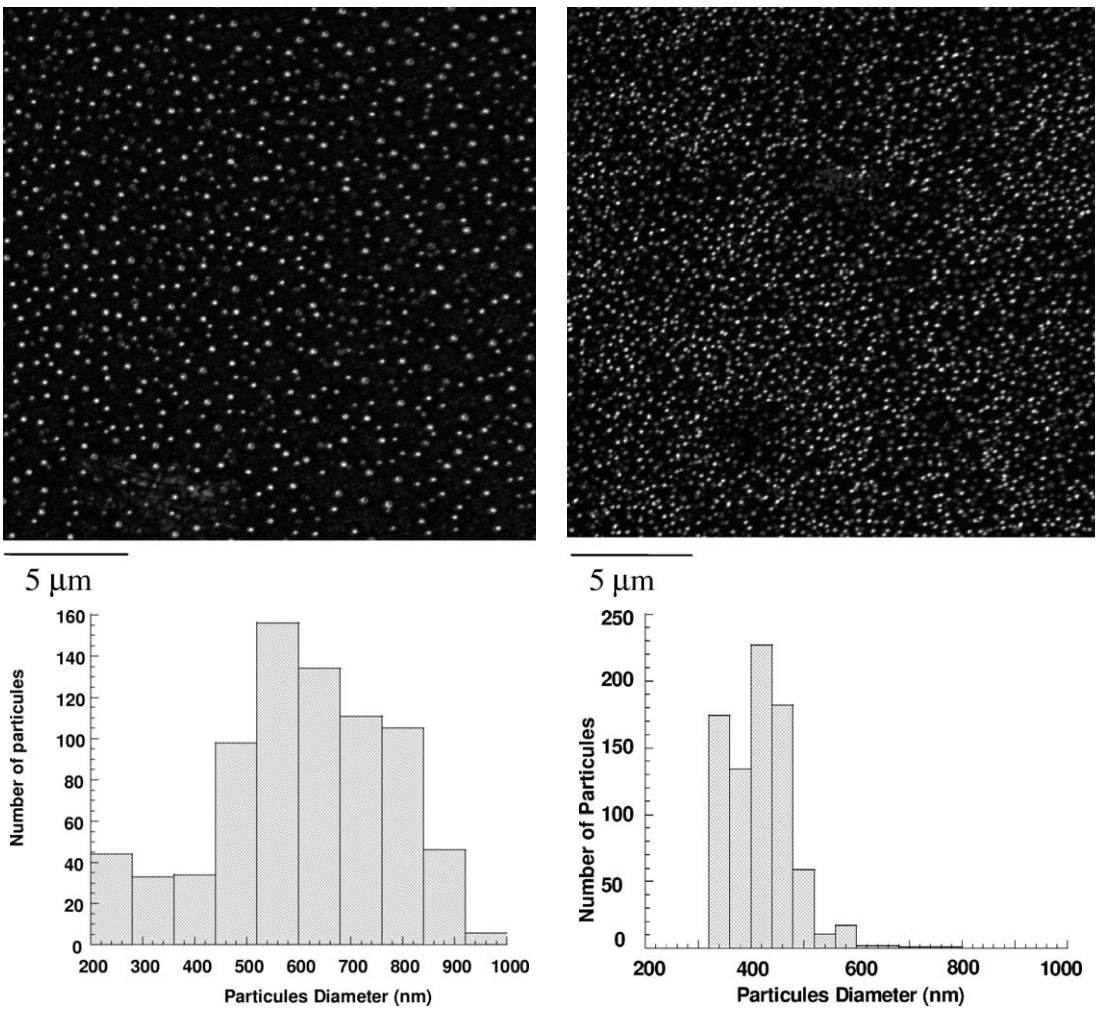

(a) (b)

Figure 9. Effect of the rotation speed, r, on the nanocrystallization of naphtalene in sol–gel thin films illustrated through confocal microscope images (reflection imaging) and their corresponding size nanocrystal histograms determined with the NIH Image Software: (a) $r = 500$ rpm; (b) $r = 4000$ rpm.

size distribution as illustrated in Fig. 9, where naphtalene crystals have been grown using rotation speeds of 4000 and 500 rpm.

Another important parameter is the nature of the solvent [15]. Its volatility is directly related to the applied supersaturation while strong dye–solvent interactions can disturb the crystallization of the organic phase, as in the case of strong dye–matrix interactions. On the other hand, the size of the particles decreases directly with dye concentration [15]. Thus, transparent thin films in the visible region can be prepared with nanocrystal sizes less than 200 nm. In this case, the particles are observed by scanning electron microscopy, Fig. 10.

Finally, atomic force microscopy shows that the thin films exhibit good surface quality with very low roughness of around 10–20 Å, because the nanocrystals are well imbedded in the sol–gel coatings [15]. Indeed, the organic nanocrystals form monolayers at the middle of the film thickness [14] and are then well

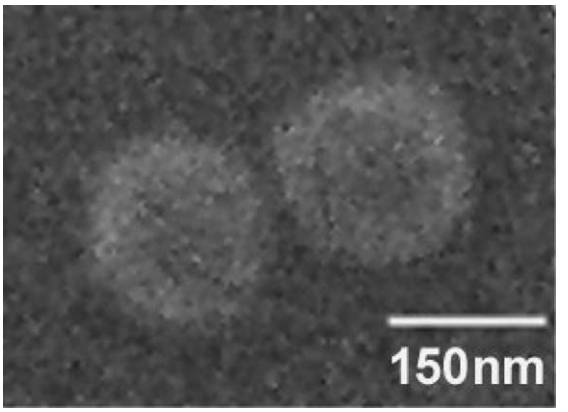

Figure 10. Scanning electron microscopy image of NPP nanocrystals grown in a TMOS + MTMOS coating.

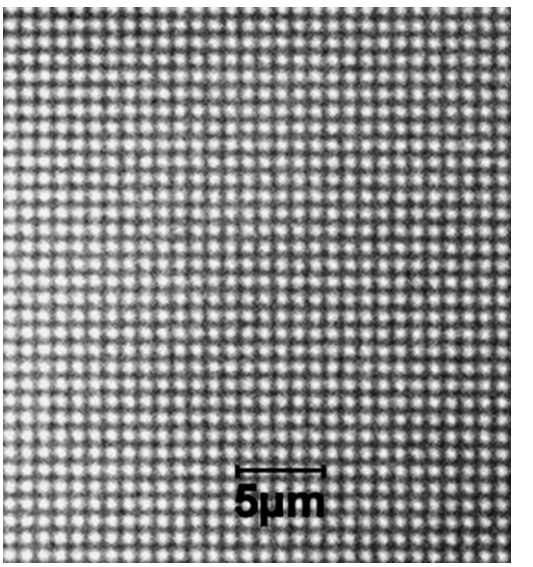

Figure 11. Confocal microscope images of a well defined 2D array of DEANST luminescent nanocrystals.

stabilized by the inorganic matrix. This resulting improved stability of the organic phase is illustrated by the fact that nanocrystals of naphtalene do not sublime significantly from the matrix. Indeed, similar confocal microscopy images (Fig. 9) are obtained several months after the coating preparation.

The targeted optical properties of these nanocomposite films, which are under characterizations, are nanocrystal spectroscopies (luminescence, photochromism and SHG) and the quenching of luminescence related to specific chemical or biological surroundings for the fabrication of sensors. We are also trying to control the poling of organic nanocrystals for electro-optical properties by applying an electric fields and thermal treatments in order to melt, then solidify the nanocrystals under the electric field. Moreover, in the last months we have undertaken the control of the spatial distribution of the nucleation sites of organic nanocrystals. Our first results are very promising as we have already observed well defined 2D arrays of DEANST luminescent nanocrystals by optical confocal microscopy, Fig. 11. We are now working on the preparation of multilayers of nanocomposite thin films involving photochromic phases in order to obtain potentially rewritable and volumic optical storage devices.

4. Conclusions and perspectives

In this work, we have designed a new type of hybrid organic–inorganic materials in order to obtain new optical properties or to improve the stability of organic molecular crystals. These materials not only combine the optical properties (nonlinear response, fluorescence, photochromism, ...) of organic molecules with those of inorganic materials (high stability, wide transparency range), but also the advantages of crystals (size effects, photostability), with those of amorphous phases (convenient processing and shaping). The validity of this simple and generic preparation of organic nanocrystals grown in gel–glasses has been demonstrated by using several types of dyes, solvents and sol–gel precursors. Particles of uniform size are obtained through the control of the nucleation of the organic phase, particle growth and gelation of the alkoxide matrix. We have greatly improved the stability (mechanical, thermal, chemical and photochemical) of the organic phases by the confined growth of the dye in the pores of dense sol–gel matrices. Nevertheless, if the dye–matrix interactions are too strong, the molecule aggregation and the crystalline structure of the resulting nanocrystals can be significantly disturbed. This route to nanocrystallites in gel–glasses offers

either bulk or thin film materials which are isotropic (randomly dispersed nanocrystals in an amorphous matrix) and contain high concentrations of dye. Our initial optical characterizations show interesting properties in the field of luminescence for high photostability sensors and in the development of optical power limiters. In order to obtain other optical properties such as quadratic NLO, electro-optic or optical data storage devices we are optimizing the control of the orientation and the spatial distribution of nanocrystals. So far, we have restricted our choice to organic molecules with optical properties, but similar hybrid nanocomposite materials could be designed with molecules exhibiting other specific properties such as magnetism.

Acknowledgments. The authors wish to thank J.F. Nicoud, IPCMS Strabourg, for his assistance in the selection of the chromophores and their preparation and Y. Usson, Institut Albert Bonniot, Univ. Grenoble I, for the collection of the optical confocal images. This research was partially supported by the French DGA and the Institut de Physique de la Matière Condensée (IPMC), Grenoble, France.

References

[1] D.S. Chemla, J. Zyss (Eds.), Nonlinear Optical Properties of Organic Molecules and Crystals, Vols. 1 and 2, Academic, Orlando, 1987.
[2] R. Masse, J. Zyss, Molec. Engng. 1 (1991) 141–152.
[3] J. Zyss, R. Masse, M. Bagieu-Beucher, J.P. Levy, Adv. Mater. 5 (1993) 120–124.
[4] J. Pécaut, R. Masse, J. Mater. Chem. 4 (1994) 1851–1854.
[5] R. Masse, Nonlinear Opt. 9 (1995) 113–126.
[6] Y. Le Fur, M. Bagieu-Beucher, R. Masse, J.F. Nicoud, J.P. Lévy, Chem. Mater. 8 (1996) 68–75.
[7] A. Ibanez, J.P. Levy, C. Mouget, E. Prieur, J. Solid State Chem. 129 (1997) 22–29.
[8] J. Zaccaro, B. Capelle, A. Ibanez, J. Cryst. Growth 180 (1997) 229–237.
[9] J. Zaccaro, J. Härtwig, J. Baruchel, A. Ibanez, J. Cryst. Growth 204 (1999) 325–332.
[10] S. Khodja, D. Josse, J. Zyss, J. Opt. Soc. Am. B 15 (1998) 751–758.
[11] J. Zaccaro, M. Chamel, A. Ibanez, J. Opt. Soc. Am. B 16 (1999) 1385–1391.
[12] N. Horiuchi, F. Lefaucheux, A. Ibanez, D. Josse, J. Zyss, Optic. Mater. 12 (1999) 351–356.
[13] J.P. Feve, B. Boulanger, I. Rousseau, G. Marnier, J. Zaccaro, A. Ibanez, IEEE J. Quantum Electron. 35 (1999) 66–71.
[14] A. Ibanez, S. Maximov, A. Guiu, C. Chaillout, P.L. Baldeck, Adv. Mater. 10 (1998) 1540–1543.
[15] N. Sanz, A.C. Gaillot, P.L. Baldeck, A. Ibanez, J. Mater. Chem. 10 (2000) 2723–2726.
[16] N. Sanz, P.L. Baldeck, A. Ibanez, Synth. Met. 115 (2000) 229–234.
[17] C.J. Brinker, G.W. Scherer, Sol–Gel Science, The Physics and Chemistry of Sol–Gel Processing, Academic Press, New York, 1990.
[18] D. Avnir, D. Levy, R. Reisfeld, J. Phys. Chem. 88 (1984) 5957–5962.
[19] D. Avnir, V.R. Kaufman, R. Reisfeld, J. Non-Cryst. Solids 74 (1985) 395–406.
[20] C. Sanchez, F. Ribot, New J. Chem. 18 (1994) 1007–1047.
[21] R. Reisfeld, Structure and Bonding, Vol. 85, Springer-Verlag, Berlin, 1996, pp. 99–145.
[22] F.S. Spano, S. Mukamel, Phys. Rev. A 40 (1989) 5783–5801.
[23] H. Ishihara, K. Cho, Phys. Rev. B 42 (1990) 1724–1730.
[24] H.S. Nalva, H. Kasai, S. Okada, H. Oikawa, H. Matsuda, A. Kakuta, A. Mukoh, H. Nakanishi, Adv. Mater. 5 (1993) 758–760.
[25] I.A. Akimov, I. Denisyuk, A.M. Meshkov, J. Opt. Spectr. 77 (1994) 858–863.
[26] Y. Komai, H. Kasai, H. Hirakoso, Y. Hakuta, H. Katagi, S. Okada, H. Oikawa, T. Adschiri, H. Inomata, K. Arai, H. Nakanishi, Jpn. J. Appl. Phys. 38 (1999) L81–L83.
[27] Y. Shen, J. Swiatkiewicz, J. Winiarz, P. Markowicz, P.N. Prasad, Appl. Phys. Lett. 77 (2000) 2946–2948.
[28] M. Bienfait, R. Kern, Bull. Soc. Française Minér. Crist. 87 (1964) 604–613.
[29] F. Lefaucheux, M.C. Robert, in: D.T.J. Hurle (Ed.), Crystal Growth in Gels, Handbook of Crystal Growth, Vol. 2b, North-Holland, Amsterdam, 1994, pp. 1271–1303.
[30] V.K. LaMer, R.H. Dinegar, J. Am. Chem. Soc. 17 (1950) 4847–4854.
[31] H. Schmidt, H. Scholze, A. Kaiser, J. Non-Cryst. Solids 63 (1984) 1–11.
[32] H. Scholze, J. Non-Cryst. Solids 73 (1985) 669–680.
[33] N. Sanz, P. Terech, D. Djurado, A. Bourret, A. Ibanez, to be published.
[34] S.N. Oliver, P. Pantelis, P.L. Dunn, Appl. Phys. Lett. 56 (1990) 307–309.
[35] G.S. He, J. Zieba, J.T. Bradshaw, M.R. Kazmierczak, P.N. Prasad, Opt. Commun. 104 (1–3) (1993) 102–106.

[36] N. Sanz, A. Boudet, A. Ibanez, J. Nanopart. Res. (2002), in press.
[37] P.A. Chollet, V. Dumarcher, J.M. Nunzi, P. Feneyrou, P.L. Baldeck, Nonlinear Opt. 21 (1999) 299–308.
[38] J. Zyss, D.S. Chemla, J.F. Nicoud, J. Chem. Phys. 74 (1981) 4800–4811.
[39] J. Zyss, J.F. Nicoud, M. Coquillay, J. Chem. Phys. 81 (9) (1984) 4160–4167.
[40] A. Boudet, L.P. Kubin, Ultramicrosc. 8 (4) (1982) 409–416.
[41] F.G. Shi, J. Mater. Res. 9 (5) (1994) 1307–1313.
[42] Z. Zhang, X.X. Lü, Q. Jiang, Phys. B 270 (3–4) (1999) 249–254.
[43] N. Sanz, J. Zaccaro, L. Delmotte, C. Le Luyer, J. Solid Stat. Chem. 165 (2002) 25–34.
[44] N. Sanz, P.L. Baldeck, J.F. Nicoud, Y. Le Fur, A. Ibanez, Solid State Sci. 3 (8) (2001) 867–875.
[45] R. Sutherland, R. Pachter, P. Hood, D. Hagan, K. Lewis, J. Perry (Eds.), Materials for Optical Limiting II, MRS Proceedings, Vol. 479, 1998.
[46] J.W. Perry, K. Mansour, I.S. Lee, X.L. Wu, P.V. Bedworth, C.T. Cheng, S.R. Marder, P. Miles, T. Wada, M. Tian, H. Sasabe, Science 273 (1996) 1533–1536.
[47] P.L. Baldeck, Y. Morel, C. Andraud, J.F. Nicoud, A. Ibanez, Photon. Sci. News 4 (1999) 5–8.
[48] P.L. Baldeck, Y. Morel, M. Plazanet, P. Feneyrou, D. Block, C. Andraud, T. Brodin, C. Nguefack, J.F. Nicoud, A. Ibanez, in: SPIE Proceedings, Vol. 3147, 1997, pp. 112–117.
[49] A.E. Mikelson, Ya.Kh. Karklin, J. Cryst. Growth 52 (1981) 524–529.
[50] G. Sazaki, E. Yoshida, H. Komatsu, T. Nakada, S. Miyashita, K. Watanabe, J. Cryst. Growth 173 (1997) 231–234.
[51] J.P. Astier, S. Veesler, R. Boistelle, Acta Cryst. D 54 (1998) 703–708.
[52] M. Ataka, E. Katoh, N.I. Wakayama, J. Cryst. Growth 173 (1997) 592–596.
[53] N. Sanz, I. Wang, J. Zaccaro, E. Beaugnon, P.L. Baldeck, A. Ibanez, Adv. Func. Mater. 12 (5) (2002).
[54] M. Barzoukas, D. Josse, P. Fremeaux, J. Zyss, J.F. Nicoud, J.O. Morley, J. Opt. Soc. Am. B 4 (6) (1987) 997–1086.
[55] S. Bénard, P. Yu, Adv. Mater. 12 (2000) 48–50.